PHYSICAL REVIEW A **73**, 041605(R) (2006)

Bragg spectroscopy of vortex lattices in Bose-Einstein condensates

S. R. Muniz,* D. S. Naik, and C. Raman
School of Physics, Georgia Institute of Technology, Atlanta, Georgia 30332, USA
(Received 12 August 2006; published 17 April 2006)

We have measured the velocity field of a vortex lattice within a sodium Bose-Einstein condensate using Bragg scattering. The phase gradient of the macroscopic wave function was mapped into the spatial structure of the diffracted atom cloud, allowing for the single shot measurement of the rotation parameters. A combination of spectral and spatial information yields a complete description of the superfluid flow, coarse grained over the lattice structure, including direct and independent measurements of the rate and sense of rotation. Signatures of the microscopic quantum rotation have also been observed.

DOI: 10.1103/PhysRevA.73.041605 PACS number(s): 03.75.Lm, 03.75.Nt, 32.80.Lg, 32.80.Pj

Vortices are a cornerstone in the study of superfluids and have applications throughout fluid mechanics and condensed matter physics [1–3]. Recently, gaseous Bose-Einstein condensates (BEC) under rotation have become an important test bed for predictions of the behavior of quantized vortices, which form highly regular lattices [4–7]. In these gases, time-of-flight (TOF) imaging has proved instrumental for observing the rotation of the cloud through the detection of the vortex cores [see Fig. 1(b) for an example]. However, this technique only measures the superfluid density and not the phase of the macroscopic wave function. Phase measurements would provide a more complete picture of vortex states, especially useful in cases where individual vortices cannot be readily detected or where the TOF expansion dynamics might be unknown at first. In atomic gases, powerful optical and spectroscopic techniques [8–12] can be readily applied, which afford new possibilities for performing phase measurements.

In this Rapid Communication, we have used two-photon Bragg scattering to study vortex lattices in a BEC. This technique directly probes the velocity distribution of the rotating superfluid, which is the gradient of the wave-function phase. Bragg scattering has been proposed for detecting the phase singularity of a single vortex [13] and was used to measure the spatial phase of a dark soliton [14]. Earlier work [9,10,15] has explored the spectroscopic nature of this tool for condensates; however, that method requires repeated experimental runs to obtain an entire spectrum. In this Rapid Communication, we demonstrate that Bragg scattering provides a unique window into a rapidly rotating BEC through the *spatial profile* of the diffracted atoms. A significant amount of information can be gleaned from a single image [16]. In particular, one can directly extract the rate and the sense of rotation from the TOF image. We use spectral and spatial information to extract a complete picture of the two-dimensional velocity flow.

Sodium BECs were produced in a TOP trap [17] by first precooling to quantum degeneracy in an optically plugged quadrupole magnetic trap (OPT) following the procedures described in Ref. [18]. The transfer to the TOP trap was effected by ramping the plug laser intensity to zero within 200 ms, followed by the immediate turn on of a rotating bias field and an additional 1 s of equilibration. After the transfer, we typically had $1-3\times10^6$ atoms with a condensate fraction $>90\%$. We used a radial gradient $B'_\rho=12$ Gauss/cm and a bias rotation of $\omega_{\mathrm{TOP}}=2\pi\times5$ kHz. The measured transverse oscillation frequency is $\omega_\rho=2\pi\times31$ Hz, with $\omega_z=\sqrt{8}\omega_\rho$.

We produced the vortex lattice by creating a rotating elliptical asymmetry in the horizontal x-y plane of the TOP trap [7]. The outputs of two frequency synthesizers were split, phase shifted, and summed together, resulting in a slow rotation at 22 Hz ($\simeq0.7\omega_\rho$ [19]) superimposed on the fast, 5 kHz rotation of the TOP field. The rotation was applied for 1.5 s and the cloud equilibrated for an additional 1–1.5 s in the radially symmetric TOP trap. This procedure reliably created lattices with approximately 40 ± 10 vortices, as shown in Fig. 1(b).

After the lattice had equilibrated, we pulsed the Bragg diffracting beams along the x direction [see Fig. 1(a)] for a time T_B, while the atoms were still in the trap. The Bragg beams were detuned by 1.7 GHz from the $F=1$ to $F'=2$ resonance, and were created by back-reflecting a single beam containing two frequencies ω_L and $\omega_L+2\pi\delta$. δ is the frequency difference between two rf synthesizers used to drive a single acousto-optic modulator. The result was a moving

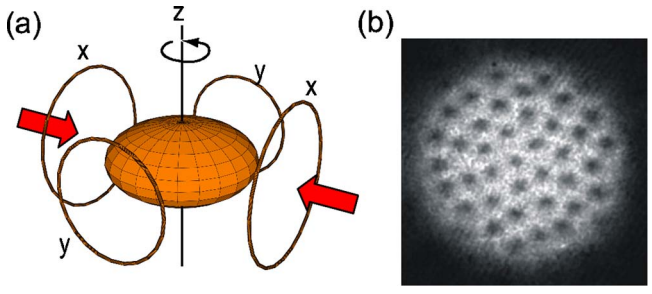

FIG. 1. (Color online) Bragg scattering from vortex lattices. (a) Atoms in a TOP trap are made to rotate about the z axis by phase control of the transverse fields produced in coil pairs x and y. This procedure forms a lattice of quantized vortices (b), which is imaged in TOF after 40 ms. The field of view is 0.6 mm. The Bragg beam containing frequencies ω and $\omega+\delta$ is applied along the x direction and retroreflected as shown in (a).

*Electronic address: sergio.muniz@physics.gatech.edu

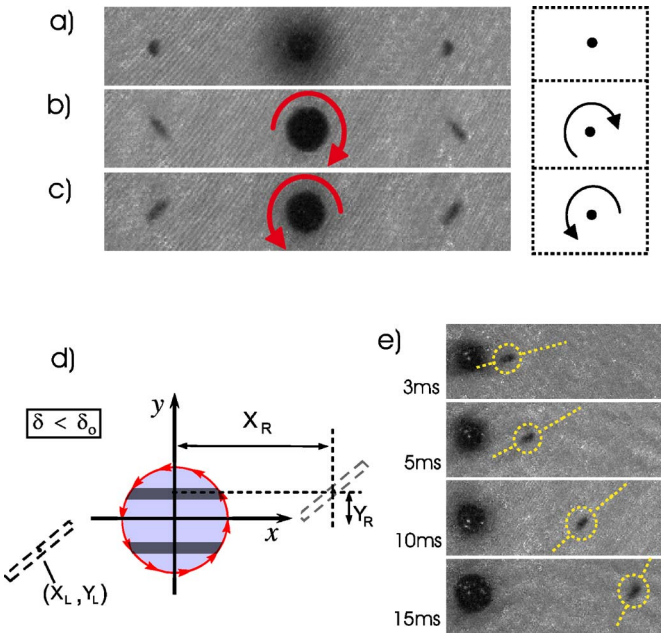

FIG. 2. (Color online) Vortices probed by Bragg scattering. Outcoupled atoms (to the far right and left of each image) showed no particular structure for nonrotating clouds (a); whereas, from vortices (b) and (c), the outcoupled atoms were tilted according to the direction of rotation. Also in (a), the higher atomic density causes collisional-induced heating and makes the cloud look more diffuse. Images (a)–(c) were taken at 10 ms TOF. The tilt angle increases with respect to TOF, as shown in (e). Each pair of Bragg frequencies is resonant with a thin strip of atoms parallel to the x axis, as illustrated in (d). All images were taken at $\delta=102$ kHz.

optical lattice that produced two diffracted (outcoupled) clouds of atoms, one with momentum $+\mathbf{q}$ and the other with $-\mathbf{q}$. In the free particle regime, the Bragg resonance condition (energy-momentum conservation) is given by $\delta_o^{fp}=\frac{q^2}{2mh}+\frac{\mathbf{q}\cdot\mathbf{v}}{h}$. The second term in δ_o^{fp} is simply the Doppler shift, which makes the Bragg technique velocity sensitive. For sodium atoms near the principal resonance, $\frac{q^2}{2mh}=100$ kHz. For a trapped BEC, one also has to consider the effects of interactions. In the mean-field and local density approximations [20,21], this causes an extra $\delta_{MF}=\frac{4\mu}{7h}$ frequency shift [9]. In our case, for a stationary condensate, the Bragg resonance is peaked at a frequency $\delta_o=\frac{q^2}{2mh}+\delta_{MF}\approx 101$ kHz. $q=|\mathbf{q}|=2h/\lambda$ is the transferred momentum, μ is the chemical potential, m and v are the atomic mass and velocity.

We applied a square-shape Bragg pulse with $T_B=250$ μs and then turned off the magnetic trap within 100 μs. The atoms were allowed to expand for a variable TOF t_{TOF} before taking an absorption image using laser light resonant with the $F=1\rightarrow 2$ transition in a 250 μs pulse. Figure 2 shows our main result—we can clearly observe *spatial structures* in the outcoupled atom cloud arising from the rotation of the lattice. Figure 2(a) shows the diffraction from an initially stationary condensate, and the outcoupled atoms appear to the right and left of the stationary condensate. No particular structure is visible. However, in Fig. 2(b), we have initially prepared a vortex lattice, which causes the diffracted atoms to form a tilted, elongated spatial pattern. Moreover, when we reversed the direction of the applied rotation (by replacing $\omega_{AR}\rightarrow-\omega_{AR}$), the tilt angle with respect to the y direction reverses, as shown in Fig. 2(c).

We can understand our observations in terms of a simple picture of rigid-body rotation, which applies for condensates containing a large number of vortices. The classical behavior results from a coarse-grained average over the velocity field of several vortices. Even though locally the tangential velocity around each core axis varies $\propto 1/r$, the bulk fluid velocity follows $v=\Omega r$, with $\Omega=|\vec{\Omega}|$ proportional to the number of vortices.

The Bragg process selects a group of atoms with the same projection of velocity v_x along the direction of the momentum transfer. In the rigid-body limit, since $v_x=\Omega y$, the resonance condition is given by $\delta=\delta_o+2y\Omega/\lambda$. Therefore, for a spectrally narrow Bragg pulse, with $\delta<\delta_o$ and a counterclockwise rotation, the resonance corresponds to a thin, horizontal band of atoms with $y>0$ for atoms, which are Bragg scattered to the right, and $y<0$ for atoms scattered to the left [the dark shaded regions in Fig. 2(d)]. In ballistic expansion, v_y results in a tilted stripe whose angle increases with time, as observed in Fig. 2(e). At a long TOF the stripe should become fully stretched along the vertical axis of the images.

According to this model, the vertical position of the center of mass for the right (left) diffracted cloud Y_R (Y_L) is set by the Bragg resonance condition and should depend on the detuning δ. Similarly, the horizontal position X_R (X_L) is given by $(\mathbf{q}\cdot\hat{\mathbf{x}}/m+v_x)t_{\mathrm{TOF}}$ and, due to its dependence on v_x, it also depends on δ. As a result, for a clockwise rotation and $(\delta-\delta_o)<0$, we should have $Y_R<0$ and $Y_L>0$. These predictions are clearly verified in Fig. 3(a), for $t_{\mathrm{TOF}}=10$ ms, at $(\delta-\delta_o)=-10$ kHz. For $\delta=+10$ kHz, the opposite is true, namely, $Y_R>0$ and $Y_L<0$, as seen in Fig. 3(b). The coordinate pair (X,Y) is the center of mass of the diffracted atom cloud within each image, as determined from a parabolic Thomas-Fermi (TF) fit to the data.

It is straightforward to show that the relative displacements between each scattered group are given by $\Delta Y=(Y_R-Y_L)=\frac{\lambda}{\Omega}(\delta-\delta_o)$ and $\Delta X=(X_R-X_L)=2\left[\frac{2h}{\lambda m}+\frac{\lambda}{2}(\delta-\delta_o)\right]t_{\mathrm{TOF}}$. Figures 3(c)–3(e) show that our measurements are in very good agreement with the expected linear behavior for this model. In particular, while Fig. 3(c) is simply a measure of the Doppler sensitivity of the technique, Figs. 3(d) and 3(e) clearly manifest the rigid-body rotation of the cloud. Furthermore, Fig. 3(e) provides the complete mapping of the velocity profile of the condensate. The straight-line dependence of ΔY vs ΔX is a direct consequence of the velocity field $\vec{v}=\vec{\Omega}\times\vec{r}$. We note that the reduced number of atoms matching the resonance condition near each vortex core makes the absorption signal below the detection limit of our image system, and as a result we do not observe the contribution of individual vortices in our measurements.

A least-square linear fitting of the data in Fig. 3(e) leads to a macroscopic angular frequency $\Omega=2\pi(14.9\pm0.8$ Hz). We also calculated the rotation frequency from the evolution of the tilt angle as a function of time [see Fig. 2(e)], $\theta(t)=\arctan(\Omega t)$, resulting in $\Omega=2\pi(15.4\pm1.1$ Hz). In addition, we used a third independent method to estimate Ω, based on the total quantized vorticity of the lattice. For that we noted

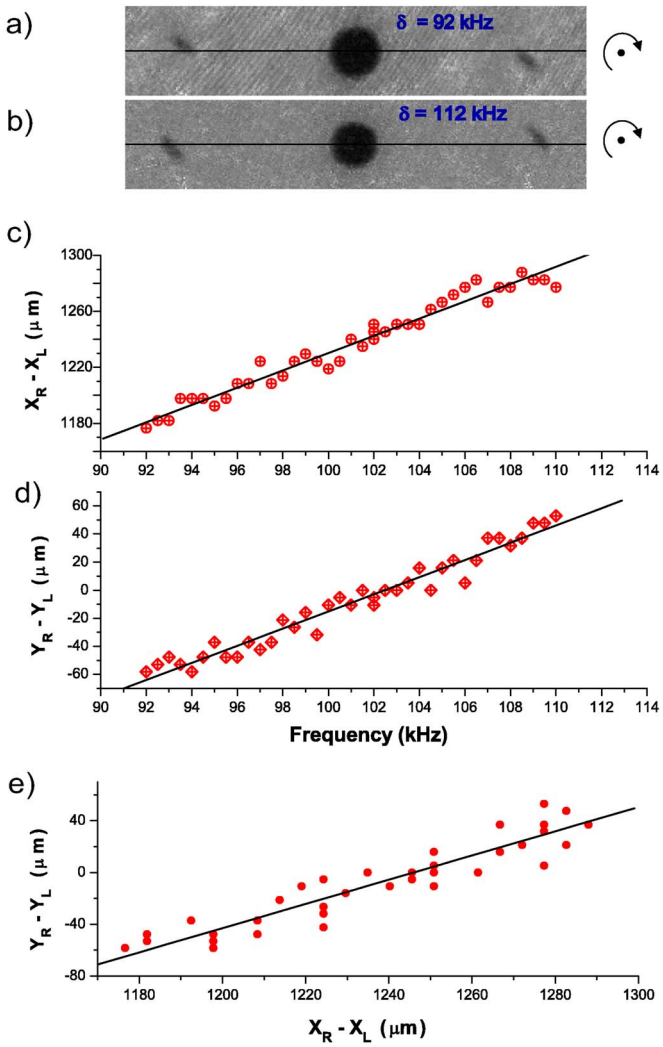

FIG. 3. (Color online) Mapping the velocity field of a vortex lattice. Measuring the center-of-mass locations of the right and left diffracted atoms $[(X_R, Y_R)$ and (X_L, Y_L), respectively, as defined in Fig. 2] in the x-y plane allows us to reconstruct the velocity profile of the rotating cloud. For negative detuning, as in (a), $\delta - \delta_0 = -10$ kHz; therefore, $Y_L > 0$ and $Y_R < 0$. For positive detuning, the opposite is the case, as in (b) where $\delta - \delta_0 = +10$ kHz. The difference $X_R - X_L$ is mapped as a function of frequency in (c), while $Y_R - Y_L$ is plotted in (d). Finally, in (e), we have plotted $Y_R - Y_L$ vs $X_R - X_L$ for the data in (c) and (d). The data in (e) are a direct map of the position (Y coordinate) vs velocity (X coordinate) distribution within the vortex lattice, and shows a linear relationship consistent with rigid-body rotation. The lines are fits to the data.

the fact that in the rigid-body limit $\Omega = (hN_V)/(2m\pi R_\rho^2)$; therefore, by measuring the number of vortices N_V, one can calculate the rotation rate. In our case $R_\rho = 35$ μm is the calculated TF radius in the x-y plane, and N_V was determined by a manual counting of the number of vortices from several images taken at long TOF. This resulted in $N_V = 37 \pm 7$, which leads to $\Omega = 2\pi(13.3 \pm 2.6$ Hz). An apparent undercounting in the number of vortices has also been previously noted in Ref. [22] and appears to be consistent with some numerical and analytical calculations [23,24]. All the methods produced similar results for Ω and indicate that the condensate was not

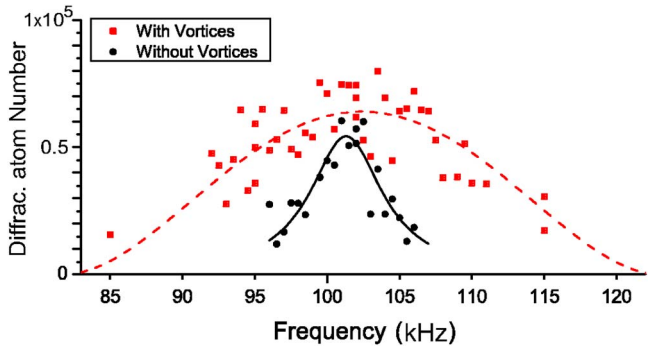

FIG. 4. (Color online) Spectroscopy of the vortex lattice. The number of Bragg diffracted atoms is measured as a function of the frequency δ, for samples with (solid circles) and without (squares) vortices. A significant broadening of the spectrum is observed in the presence of vortices due to the broad velocity distribution caused by the rigid-body rotation. The solid curve represents the best Lorentzian fit to the data, while the dashed curve refers to the model described in the text.

completely equilibrated with the rotating potential at frequency ω_{AR}. However, we observed that the vortex number decreased for longer rotation times, probably due to residual asymmetry in the trapping frequencies of our TOP trap.

In addition to this spatial analysis, we can also use Bragg spectroscopy to derive information about the velocity profile from the *number* of outcoupled atoms [9,14]. We measured this number as a function of the frequency δ, with and without vortices present in the system. Figure 4 shows the result for both cases. We observed a significant Doppler broadening of the spectrum in the presence of vortices as a result of the rotation, which was investigated in Fig. 3.

In order to accurately reconstruct the velocity field, one needs a narrow spectral resolution. The initial width of the diffracted stripe is determined by the Bragg resonance linewidth and can be affected by several broadening mechanisms [21,25]. Our results in Fig. 4 (*solid circles*) show a rms width of 3 kHz for a nonrotating condensate, consistent with the residual Doppler shifts due to condensate sloshing (measured to be ~ 800 μm/s) and the other broadening mechanisms [26].

We can calculate the theoretical spectrum by noting that the total number of diffracted atoms at frequency δ is proportional to the area within the left- and right-moving slices for $y = \frac{\lambda(\delta - \delta_o)}{2\Omega}$, as defined in Fig. 3(d). Using a TF profile for the density distribution and integrating inside the volume defined by the corresponding TF radii, we find that the spectral line shape is $\propto \left[\left(\frac{\delta - \delta_o}{A}\right)^2 - 1\right]^2$, where $A = 2\Omega R/\lambda$. The rms width of this distribution is $W_{\rm rms} = 0.38 \times A$, and a fit of the data (*squares*) in Fig. 4, for $|\delta - \delta_o| \leq A$, yields $W_{\rm rms} = 7.5$ kHz. We can compare this with the theoretical estimate for W obtained using $\Omega = 2\pi \times 16$ Hz, as measured from the data in Fig. 3 and $R = 35$ μm. When convolved with the experimental rms resolution of 3 kHz observed for nonrotating clouds, this yields $W_{\rm rms} = 5.4$ kHz.

A rigidly rotating classical body has a uniform distribution of vorticity, while for a rotating quantum fluid the vorticity is concentrated in individual cores. The spatial profile

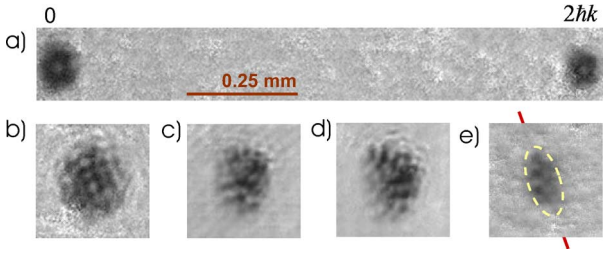

FIG. 5. (Color online) Microscopic structures seen in Bragg scattered clouds. A $T_B=20$ μs pulse $\delta=102$ kHz was used in (a), in a single vortex condensate (at the left side of the image). The sequences (b)–(e) show detailed images of outcoupled clouds for rapidly rotating (full lattice) condensates. Experimental parameters are $T_B=75$ μs, $\delta=102$ kHz in (b); $T_B=60$ μs, $\delta=102$ kHz in (c); $T_B=60$ μs, $\delta=122$ kHz in (d); and $T_B=50$ μs, $\delta=115$ kHz in (e). For all images, TOF=20 ms. An interesting combination of the quantum (microscopic structures) and classical (rigid-body tilting) superfluid flow is shown in (e).

of the Bragg scattered atoms should contain evidence of the quantum nature of the rotation. In Fig. 5(a), we have observed this quantum signature—the diffracted atom cloud shows a distinct density minimum correlating with that present in the undiffracted atoms. We obtained this image by holding the rotating BEC for 10 s until only 1–2 vortices remained in the gas and by using a short, 20 μs Bragg pulse with a corresponding broad velocity spread of 2.4 mm/s. In this limit, the spatial structure of the diffracted atoms is more closely related to the original density profile than to the velocity distribution. Unlike the TOF images in Fig. 1(a), these are subject to additional blurring due to the motion of the recoiling atoms during the Bragg pulse; therefore, the cores have lower contrast. We could also observe vortex signatures corresponding to an entire lattice, as shown in Figs. 5(b)–5(e). A particularly interesting one is Fig. 5(e) where one can see in the same image a combination of quantum and classical fluid behavior. However, the TOF expansion dynamics of the scattered atoms are quite complex due to the mean-field interaction with the undiffracted condensate. Therefore, while these signatures are intriguing, care must be taken to correlate them with the microscopic structure of the original rotating BEC.

In conclusion, Bragg scattering was used to directly measure the velocity profile of a rotating BEC and to observe signatures of its quantized vortex structure. While the classical flow is readily understood, further understanding of the TOF dynamics is necessary to provide a quantitative account of the microscopic velocity field.

We thank Brian Kennedy and Leslie Baksmaty for a critical reading of the manuscript and Michael Chapman for loaning a frequency synthesizer. This work was supported by the U.S. Department of Energy, the Army Research Office, and by Georgia Tech.

[1] R. J. Donnelly, *Quantized Vortices in Helium II* (Cambridge University Press, Cambridge, U.K., 1991).
[2] C. F. Barenghi, R. J. Donnelly, and W. F. Vinen, *Quantized Vortex Dynamics and Superfluid Turbulence* (Springer, Berlin, 2001).
[3] D. R. Nelson, *Defects and Geometry in Condensed Matter Physics*, 1st ed. (Cambridge University Press, Cambridge, U.K., 2001).
[4] K. W. Madison, F. Chevy, W. Wohlleben, and J. Dalibard, Phys. Rev. Lett. **84**, 806 (2000).
[5] J. R. Abo-Shaeer *et al.*, Science **292**, 476 (2001).
[6] P. C. Haljan, I. Coddington, P. Engels, and E. A. Cornell, Phys. Rev. Lett. **87**, 210403 (2001).
[7] E. Hodby, G. Hechenblaikner, S. A. Hopkins, O. M. Marago, and C. J. Foot, Phys. Rev. Lett. **88**, 010405 (2002).
[8] M. Kozuma *et al.*, Phys. Rev. Lett. **82**, 871 (1999).
[9] J. Stenger *et al.*, Phys. Rev. Lett. **82**, 4569 (1999).
[10] M. Theis *et al.*, Phys. Rev. Lett. **93**, 123001 (2004).
[11] N. Katz *et al.*, Phys. Rev. Lett. **93**, 220403 (2004).
[12] J. E. Simsarian *et al.*, Phys. Rev. Lett. **85**, 2040 (2000).
[13] P. B. Blakie and R. J. Ballagh, Phys. Rev. Lett. **86**, 3930 (2001).
[14] K. Bongs *et al.*, J. Opt. B: Quantum Semiclassical Opt. **5**, S124 (2003).
[15] S. Richard *et al.*, Phys. Rev. Lett. **91**, 010405 (2003).
[16] R. Ozeri, J. Steinhauer, N. Katz, and N. Davidson, Phys. Rev. Lett. **88**, 220401 (2002).
[17] W. Petrich, M. H. Anderson, J. R. Ensher, and E. A. Cornell, Phys. Rev. Lett. **74**, 3352 (1995).
[18] D. S. Naik and C. Raman, Phys. Rev. A **71**, 033617 (2005).
[19] K. W. Madison, F. Chevy, V. Bretin, and J. Dalibard, Phys. Rev. Lett. **86**, 4443 (2001).
[20] F. Zambelli, L. Pitaevskii, D. M. Stamper-Kurn, and S. Stringari, Phys. Rev. A **61**, 063608 (2000).
[21] P. B. Blakie, R. J. Ballagh, and C. W. Gardiner, Phys. Rev. A **65**, 033602 (2002).
[22] P. C. Haljan, Ph.D. thesis, University of Colorado, 2003.
[23] D. L. Feder and C. W. Clark, Phys. Rev. Lett. **87**, 190401 (2001).
[24] J. R. Anglin and M. Crescimanno, e-print cond-mat/0210063.
[25] D. M. Stamper-Kurn *et al.*, Int. J. Mod. Phys. B **15**, 1621 (2001).
[26] In the case of a stationary BEC, the quadrature sum of all the broadening mechanisms (mean field, the finite-pulse duration, finite-size effect, and light intensity broadening) calculated for our system is $\Delta\nu\cong 1$ kHz.